



Stevenson, A. J., Vanwalleghem, G., Stewart, T. A., Condon, N. D., Lloyd-Lewis, B., Marino, N., Putney, J. W., Scott, E. K., Ewing, A. D., & Davis, F. M. (2020). Multiscale imaging of basal cell dynamics in the functionally mature mammary gland. *Proceedings of the National Academy of Sciences of the United States of America*, 117(43), 26822-26832. <https://doi.org/10.1073/pnas.2016905117>

Peer reviewed version

Link to published version (if available):  
[10.1073/pnas.2016905117](https://doi.org/10.1073/pnas.2016905117)

[Link to publication record in Explore Bristol Research](#)  
PDF-document

This is the author accepted manuscript (AAM). The final published version (version of record) is available online via National Academy of Sciences at <https://www.pnas.org/content/117/43/26822> . Please refer to any applicable terms of use of the publisher.

## University of Bristol - Explore Bristol Research

### General rights

This document is made available in accordance with publisher policies. Please cite only the published version using the reference above. Full terms of use are available: <http://www.bristol.ac.uk/red/research-policy/pure/user-guides/ebr-terms/>

# PNAS

www.pnas.org

## Multiscale imaging of basal cell dynamics in the functionally-mature mammary gland

Alexander J. Stevenson<sup>1,2†</sup>, Gilles Vanwalleghem<sup>3†</sup>, Teneale A. Stewart<sup>1,2</sup>, Nicholas D. Condon<sup>4</sup>, Bethan Lloyd-Lewis<sup>5</sup>, Natascia Marino<sup>6,7</sup>, James W. Putney<sup>8</sup>, Ethan K. Scott<sup>3</sup>, Adam D. Ewing<sup>1,2</sup>, Felicity M. Davis<sup>1,2\*</sup>

<sup>1</sup>Mater Research Institute-The University of Queensland, Faculty of Medicine, The University of Queensland, Brisbane, Queensland, Australia.

<sup>2</sup>Translational Research Institute, Woolloongabba, Queensland, Australia.

<sup>3</sup>Queensland Brain Institute, The University of Queensland, Brisbane, Queensland, Australia.

<sup>4</sup>Institute for Molecular Bioscience, The University of Queensland, Brisbane, Queensland, Australia.

<sup>5</sup>School of Cellular and Molecular Medicine, University of Bristol, Bristol, UK.

<sup>6</sup>Susan G. Komen Tissue Bank at IU Simon Cancer Center, Indianapolis, USA.

<sup>7</sup>Department of Medicine, Indiana University School of Medicine, Indianapolis, USA.

<sup>8</sup>National Institute of Environmental Health Sciences, National Institutes of Health, Research Triangle Park, North Carolina, USA.

†Equal contribution.

\* Felicity Davis, [f.davis@uq.edu.au](mailto:f.davis@uq.edu.au) +61-7-3443-7422

0000-0001-5909-066X, 0000-0002-6188-9582, 0000-0003-4837-9315, 0000-0002-1833-1129,  
0000-0001-6511-1818, 0000-0002-3379-4789, 0000-0003-3150-9216, 0000-0002-4544-994X,  
0000-0001-9112-118X

**Classification**

BIOLOGICAL SCIENCES: Cell Biology.

**Keywords**

Calcium signaling, GCaMP6, oscillations, mammary gland, lactation, oxytocin.

**Abstract**

The mammary epithelium is indispensable for the continued survival of more than 5000 mammalian species. For some, the volume of milk ejected in a single day exceeds their entire blood volume. Here, we unveil the spatiotemporal properties of physiological signals that orchestrate the ejection of milk from alveolar units and its passage along the mammary ductal network. Using quantitative, multidimensional imaging of mammary cell ensembles from GCaMP6 transgenic mice, we reveal how stimulus evoked  $\text{Ca}^{2+}$  oscillations couple to contractions in basal epithelial cells. Moreover, we show that  $\text{Ca}^{2+}$ -dependent contractions generate the requisite force to physically deform the innermost layer of luminal cells, compelling them to discharge the fluid that they produced and housed. Through the collective action of thousands of these biological positive displacement pumps, each linked to a contractile ductal network, milk begins its passage toward the dependent neonate, seconds after the command.

**Significance Statement**

The mammary gland is functional for only a brief period of a female's lifetime. During this time, it operates not for the survival of the individual, but for the survival of her species. Here, we visualize the nature of alveolar contractions in the functionally-mature mammary gland, revealing how specialized epithelial cells, which possess the ability to behave like smooth muscle cells, undergo  $\text{Ca}^{2+}$ -dependent contractions. We demonstrate that individual oscillators can be electrically coupled to achieve global synchrony, a phenomenon that has not yet been observed in the mammary gland. By imaging activity across scales, we provide a window into the organization, dynamics and role of epithelial  $\text{Ca}^{2+}$  oscillations in the organ principally responsible for sustaining neonatal life in mammals.

## 1 Introduction

2 The mammary gland has a central role in the health and survival of all mammals (1, 2).  
3 Development of this organ is a multi-step process that begins as the female embryo develops in  
4 her mother's uterus (2, 3) and culminates as she nurtures the next generation of offspring in her  
5 own (2, 4). In mice, the post-pubertal female mammary gland consists of an elaborate network of  
6 evenly spaced branching ducts embedded within an adipocyte-rich stroma (4). Each mammary  
7 duct consists of an inner layer of heterogeneous luminal epithelial cells, which include both estrogen  
8 receptor (ER) -positive and -negative cell lineages (5, 6). These cells are surrounded by a layer of  
9 basal epithelial cells, which express the basal cytokeratins (K) -5 and -14 as well as smooth muscle  
10 actin (SMA) (7, 8). Heterogeneity also exists within the basal cell compartment, with recent single  
11 cell RNA sequencing confirming clusters of cells with high levels of the genes encoding SMA,  
12 oxytocin receptor (OXTR) and K15 (termed basal myoepithelial cells) as well as a population of  
13 cells with high levels of *Procr*, *Gng11* and *Zeb2* (termed basal *Procr*<sup>+</sup> cells) (7).

14  
15 During alveologensis in pregnancy, adult mammary stem and progenitor cells rapidly proliferate  
16 to generate the millions of new cells that are required to produce, store and expel milk during  
17 lactation (9, 10). These cells are arranged in mammary alveoli, with each alveolar unit broadly  
18 consisting of an inner layer of secretory luminal cells and an outer network of contractile basal cells  
19 (4). Many alveolar units cluster to form large lobuloalveolar complexes, which connect to each other  
20 and to the nipple via the tubular ductal network. The development and function of epithelial cells in  
21 the mammary gland during pregnancy and lactation are governed by a range of local and systemic  
22 factors (11). A greater appreciation of these factors, and the molecular pathways that link signal  
23 reception to cellular outcomes, would greatly improve our understanding of this fundamental  
24 process in mammalian biology.

25  
26 The ability to visualize how a single living cell, in its native environment, translates an extracellular  
27 message into an intracellular signal to execute a defined task at the cell level and cooperatively  
28 achieve a biological outcome at the organ level is revolutionizing our understanding of multicellular  
29 systems. Such an approach has provided new insights into a range of biological phenomena,  
30 including how plants defend against herbivory (12), how fish escape looming predators (13, 14)  
31 and how mammals store memories (15). The rational design and continued refinement of  
32 genetically-encoded  $\text{Ca}^{2+}$  indicators (GECIs) has fueled these advances (16). However, the use of  
33 GECIs for *in situ* activity mapping in adult vertebrates, has largely remained an achievement of  
34 neuroscience, where neural activity is tightly coupled to intracellular  $\text{Ca}^{2+}$  ( $[\text{Ca}^{2+}]_i$ ) signaling (17).

35

36 Efforts to map activity networks in specific populations of non-excitabile cells in other solid organs  
37 is lagging. Indeed, our understanding of signal transduction in many epithelial tissue types  
38 (including the mammary gland) has principally arisen through analysis of isolated cells (often  
39 serially propagated under physiologically extraneous conditions), retrospective examination of fixed  
40 tissue and interrogation of genetic knockout models (where biological function is inferred in the  
41 absence of physiological redundancy or compensation). The ability to visualize signal-response  
42 relationships in mammary epithelial cells *in situ* and across scales will shed important new light on  
43 both structure-function relationships and patterns of cellular connectivity in this important epithelial  
44 organ.

45

46 When young offspring suckle, maternally produced OT binds to its cognate receptor (the OXTR)  
47 on mammary basal cells, causing them to contract (18). Activity is likely to be tightly coupled to  
48  $[Ca^{2+}]_i$  in these cells via a phospholipase C (PLC)-inositol trisphosphate (InsP3) signaling pathway  
49 (18–22). The absence of physiological redundancy in the mammary OT/OXTR system—highlighted  
50 by the inability of both OT ligand- and receptor- null mice to adequately nurse their pups (23–25)  
51 (a phenotype that can be rescued in ligand null animals through administration of exogenous OT  
52 (24))—facilitates the direct visualization of this specific epithelial signal-response relationship at this  
53 important stage of development.

54

55 In this study, we engineered mice with directed expression of a GECI to basal epithelial cells in the  
56 mammary gland. This enabled us to quantitatively probe the organization and function of real-time  
57  $[Ca^{2+}]_i$  signaling events in individual cells within this complex living tissue, at a level of rigor that has  
58 only previously been achieved in the adult brain.

## 59 **Results**

### 60 **Basal cell $[Ca^{2+}]_i$ oscillations signal to repetitively deform mammary alveoli and force milk** 61 **out.**

62 We developed transgenic mice that express the fast, ultrasensitive GECI GCaMP6f (16) under the  
63 inducible control of the K5 gene promoter (8) (*GCaMP6f;K5CreERT2* mice) (Fig. 1A). The relatively  
64 high baseline fluorescence of this GECI is well suited for the quantitative assessment of  $[Ca^{2+}]_i$   
65 responses in alveolar basal cells, which are sparsely distributed with thin cellular processes (16,  
66 26) (see SI Appendix, Fig. S1A-B). GCaMP6f consists of a circularly permuted green fluorescent  
67 protein (GFP), enabling 3D assessment of its expression and lineage specific localization using an  
68 anti-GFP antibody (27) and optimized methods for tissue clearing (28). Genetic recombination in  
69 this model was high (see SI Appendix, Fig. S2A-B) and showed lineage restriction to basal epithelial  
70 cells (Fig. 1B).

71

72 To assess OT-mediated basal cell  $[Ca^{2+}]_i$  responses, we performed 4-dimensional ( $x$ -,  $y$ -,  $z$ -,  $t$ -)  
73 imaging of *ex vivo* mammary tissue pieces from lactating *GCaMP6f;K5CreERT2* mice—a method  
74 similar to the preparation of acute brain slices for neural imaging (see Methods) (29). Tissue was  
75 loaded with the live cell permeable dye CellTracker™ Red to visualize alveolar luminal (milk  
76 producing) cells (see SI Appendix, Fig. S1A). A coordinated wave of  $[Ca^{2+}]_i$ , due to InsP3-mediated  
77 endoplasmic reticulum (ER)  $Ca^{2+}$  store release (18, 19, 22), was observed in mammary basal cells  
78 following OT stimulation and its diffusion through the tissue (Fig. 1C and Movie S1). This initial  
79 transient  $[Ca^{2+}]_i$  elevation was followed by a phase of stochastic  $[Ca^{2+}]_i$  oscillations (Fig. 1C  
80 arrowheads and Movie S1) that were likely to be sustained in-part by  $Ca^{2+}$  influx across the plasma  
81 membrane (19, 21, 30).

82

83 The organization of basal cell contractions was also examined using 3-dimensional, deep tissue  
84 imaging of myosin light chain (MLC) phosphorylation. In tissue treated with OT prior to fixation,  
85 phospho-MLC (pMLC) -positive and -negative basal cells were observed to be interspersed  
86 throughout alveolar clusters (Fig. 1D), supporting the ostensibly stochastic nature of the mammary  
87 contractile response. Regions containing clusters of pMLC-positive cells, however, were also  
88 observed in OT treated tissue (see SI Appendix, Fig. S3A asterisk and S3B). Intravital imaging of  
89 OT-mediated  $[Ca^{2+}]_i$  responses (31), supported observations in acute *ex vivo* tissue preparations  
90 (see SI Appendix, Fig S4A-C and Movie S2).

91

92 To determine whether increases in  $[Ca^{2+}]_i$  are temporally correlated with alveolar unit contractions  
93 we quantified  $Ca^{2+}$ -contraction responses in alveolar tissue. Whilst cell- and tissue- level movement  
94 is physiologically relevant and important, it poses additional computational challenges to the  
95 analysis of single cell  $Ca^{2+}$  responses in 4D image sequences. To overcome this, we utilized the  
96 diffeomorphic registration approach of Advanced Normalization Tools for motion correction (32, 33)  
97 (see Methods). This approach corrected major tissue movements, however, alveolar unit  
98 contractions remained largely intact, enabling quantification of  $[Ca^{2+}]_i$  responses in basal cells and  
99 analysis of the physical distortions to the alveolar units that these cells embrace. These analyses  
100 confirmed that increases in  $[Ca^{2+}]_i$  in individual basal cells were temporally correlated with physical  
101 distortions to the mechanically compliant luminal cell layer (Fig. 1E and see SI Appendix, Fig. S5A).  
102 For both the first InsP3 response and the subsequent oscillatory phase, increases in  $[Ca^{2+}]_i$   
103 preceded alveolar unit contractions (Fig. 1F-G and see SI Appendix, Fig. S5B). No statistical  
104 difference in the firing interval for  $[Ca^{2+}]_i$  was observed between the first and second events and all  
105 subsequent events (Fig. 1H). No  $[Ca^{2+}]_i$  oscillations or contractions were observed in live tissue in  
106 the absence of OT stimulation (see SI Appendix, Fig. S5C). These results reveal that each

107 mammary alveolar unit, acting downstream of a basal cell OT-OXTR-InsP3-Ca<sup>2+</sup> signaling axis,  
108 serves as a biological positive-displacement pump, repeatedly forcing milk out of its central lumen  
109 for passage through the ductal network.

### 110 **Basal cell contractions are Ca<sup>2+</sup> signal dependent**

111 To directly assess Ca<sup>2+</sup>-contraction coupling in mammary basal cells, we engineered triple  
112 transgenic mice that express GCaMP6f and the red fluorescent protein TdTomato (34) in basal  
113 cells (*GCaMP6f-TdTom;K5CreERT2* mice) (Fig. 2A). Using this model, we observed large  
114 increases in [Ca<sup>2+</sup>]<sub>i</sub> in single TdTomato-positive basal cells in response to OT, which immediately  
115 preceded their contraction (Figs. 2A-C and see SI Appendix, Fig. S6 and Movie S3). These data  
116 reveal with greater optical clarity how basal cells contract to deform the inner luminal cell layer for  
117 milk ejection and show unequivocally, using a second model to measure basal cell contraction, a  
118 temporal relationship between the Ca<sup>2+</sup> signal and the contractile response (see SI Appendix, Fig.  
119 S6B).

120

121 To determine whether Ca<sup>2+</sup> forms an essential component of the signal transduction pathway  
122 linking OXTR engagement to basal cell contraction, we examined [Ca<sup>2+</sup>]<sub>i</sub> and contraction events  
123 under extracellular Ca<sup>2+</sup>-free conditions. Tissue was isolated from pregnant *GCaMP6f-*  
124 *TdTom;K5CreERT2* mice and incubated in Ca<sup>2+</sup>-free physiological salt solution supplemented with  
125 the Ca<sup>2+</sup> chelator BAPTA. By performing experiments using mammary tissue harvested prior to  
126 secretory activation (gestation day 15.5-16.5), when Ca<sup>2+</sup>-contraction coupling is observed (Movie  
127 S4), we were able to avoid the exceedingly high (> 90 mM) extracellular Ca<sup>2+</sup> concentrations  
128 present in secreted milk (19). Under these experimental conditions, addition of OT resulted in  
129 intracellular Ca<sup>2+</sup> store release associated with cell contraction (Fig. 2D-E and Movie S5). Ensuing  
130 spike trains, however, were absent and subsequent contractions were abolished. Re-addition of  
131 extracellular Ca<sup>2+</sup> led to the resumption of Ca<sup>2+</sup> firing and basal cell contractions (Fig. 2D-F). These  
132 data demonstrate that both Ca<sup>2+</sup> release from InsP3-sensitive intracellular Ca<sup>2+</sup> stores (22) and  
133 Ca<sup>2+</sup> influx across the plasma membrane are sufficient for basal cell contraction but that influx  
134 across the membrane is necessary to sustain cell and tissue contractions.

### 135 **Both ducts and alveoli contract to expel milk in the mature gland**

136 The lactating mouse mammary gland consists of milk producing alveoli that are connected to the  
137 nipple via a branching ductal network (Fig. 1A). Heterogeneity in the expression of contractile  
138 markers in basal cells of ducts and alveoli has led to speculation that these two related (but  
139 spatially- and morphologically-distinct) cell populations are functionally divergent (35). We  
140 compared expression of myosin light chain kinase (MLCK), calponin (CNN1) and caldesmon  
141 (CALD1)—key components of the vascular smooth muscle contraction pathway that are



142 upregulated in the mammary gland during lactation (see SI Appendix, Fig. S7)—in ducts versus  
143 alveoli of lactating mice (Fig. 3A) and humans (Fig. 3B). Our analyses reveal that these proteins  
144 are expressed at comparable levels in basal cells of both structures (Fig. 3A-B and see SI  
145 Appendix, Fig. S8).

146

147 Next, we used our model to examine possible  $\text{Ca}^{2+}$ -contraction coupling in ductal cells of pregnant  
148 *GCaMP6f-TdTom;K5CreERT2* mice. At this developmental stage, contractile proteins are already  
149 upregulated (see SI Appendix, Fig. S7C),  $\text{Ca}^{2+}$ -contraction coupling is observed in alveolar  
150 structures (Movies S4-5) and the visualization of ducts is not completely obscured by light scattering  
151 and/or absorptive properties of interposing structures. Although oriented deep within the tissue,  
152 ductal basal cells responded to OT with a transient increase in  $[\text{Ca}^{2+}]_i$  (Fig. 3C) and  $\text{Ca}^{2+}$ -contraction  
153 coupling was clearly observed in live recordings (Movie S6). Although more challenging to  
154 visualize, large ducts that were positioned deep within the mammary tissue of lactating animals  
155 were captured (Fig. 3D and Movie S7), confirming these findings in the fully mature state. In  
156 mammary ducts, basal cells adopt a spindle-like morphology and are collectively oriented along the  
157 length of the duct (Fig. 1A). Our data reveal that contraction of ductal basal cells generates  
158 longitudinal motion, facilitating the continued flow of milk. We also demonstrate that differences in  
159 the type of motion generated by ductal and alveolar contractions arise from organizational  
160 heterogeneity—rather than divergent functional differentiation or signal transduction.

### 161 **Mammary epithelial cells *in situ* exhibit both stochastic and coordinated behaviors**

162 Our model enables us to visualize molecular events in single cells, to observe how these events  
163 control an individual cell's behavior and to understand how individual behaviors produce tissue-  
164 level outcomes. In mammary tissue, basal epithelial cells primarily exhibit stochastic activity (Figs  
165 1-2 and see SI Appendix, Figs S4-5). Individual oscillatory behavior, however, was observed to be  
166 temporarily entrained across large lobuloalveolar structures (Fig. 3C asterisks and see SI  
167 Appendix, Figs S3-4 asterisks and Movies S2, S4 and S6), suggesting that this organ can generate  
168 both synchronized and unsynchronized motion for optimal milk ejection. To determine the degree  
169 of lobuloalveolar cooperativity in firing, we employed two agnostic approaches to analyze the  
170 functional connectivity in  $\text{Ca}^{2+}$  signaling events. First, we analyzed correlations in the firing pattern  
171 of individual basal cells in the post diffusion phase and graphed the Euclidean distances between  
172 highly correlated ( $> 0.5$ ) cells. Highly correlated responses exhibited a short Euclidean distance  
173 (Fig. 3E). We also analyzed network topologies by connecting highly correlated cells within a single  
174 field-of-view. This method confirmed high clustering associated with short internodal distances in

175 some lobular structures (small worldness) (see SI Appendix, Fig. S9) (36, 37). These analyses  
176 suggest some cooperativity in firing and, by extension, contraction.

### 177 **Distinct signaling pathways underpin the passage of milk, tears and sperm**

178 To assess potential conservation in the signaling pathways that operate in basal cells of other OT-  
179 sensitive, fluid transporting epithelia, we assessed OT-mediated responses in the lacrimal glands  
180 and epididymides of *GCaMP6f-TdTom;K5CreERT2* mice. In the lacrimal gland, basal cells have a  
181 similar morphology, arrangement and function to mammary basal cells (38). They have previously  
182 been shown to undergo OT-dependent contractions (39), and diminished OT-OXTR signaling in  
183 these cells has been linked to dry eye disease (39). Like the mammary gland, dual expression of  
184 basal and smooth muscle markers was confirmed in lacrimal acini (Fig. 4A), however, no OT-  
185 mediated  $[Ca^{2+}]_i$  or contractile responses were detected in these cells in this study (Fig. 4B-C and  
186 Movie S8).

187

188 In males, a large burst of OT is released into the bloodstream at ejaculation (18, 40). This produces  
189 contractions of the male reproductive tract and, by assisting with the passage of fluid along this  
190 tract, these contractions are thought to reduce post-ejaculatory refractoriness and improve  
191 reproductive readiness (40, 41). Epididymal basal cells express basal cell markers, however, unlike  
192 the lacrimal and mammary glands, they do not co-express smooth muscle markers (Fig. 4D).  
193 Instead, movement of fluid through this organ appears to rely on a layer of smooth muscle  
194 surrounding the inner tubular epithelium (Fig. 4D). To assess the transport of sperm through this  
195 organ, its OT-responsiveness and its relationship to basal cell  $[Ca^{2+}]_i$  elevations, we stimulated  
196 acute epididymal tissue pieces with a large bolus dose of OT. OT stimulation triggered marked  
197 peristaltic-like movements of the epididymal tubes (Fig. 4E) and a supra-basal pattern of  
198 phosphorylation of MLC (see SI Appendix, Fig. S10A). Low frequency  $Ca^{2+}$  firing in basal cells was  
199 observed before and after OT-stimulation (Figs 4F arrows and see SI Appendix, S10B and Movie  
200 S9). Basal cell  $Ca^{2+}$ -contraction signaling can therefore be selectively uncoupled in different fluid  
201 moving epithelia.

202

### 203 **Pharmacological inhibitors of regulatory proteins of myosin light chain phosphorylation are** 204 **unable to block mammary contractions**

205 Mammary basal cells typically express smooth muscle actin (see SI Appendix, Fig. S1A) and  
206 strongly upregulate elements of the vascular smooth muscle contraction pathway during gestation  
207 and early lactation (see SI Appendix, Fig. S7) (7). Our group and others have therefore  
208 hypothesized that basal cell contraction is principally controlled by  $Ca^{2+}$ /calmodulin-dependent  
209 phosphorylation of the myosin light chain (MLC) by MLCK and subsequent de-phosphorylation by  
210 myosin light chain phosphatase (MLCP) (19, 20, 42). This hypothesis is supported in the current

211 study by a pattern of pMLC immunostaining in OT-treated tissue that is consistent with the  
212 organization of its  $\text{Ca}^{2+}$  firing activity (Fig. 1C-D and see SI Appendix, Fig. S3). To explore this  
213 further, we treated uterine, bladder, epididymal and mammary tissue pieces with pharmacological  
214 inhibitors of both MLCK and the MLCP inhibitor rho-associated protein kinase (ROCK) (see SI  
215 Appendix, Fig. S11A). Inhibition of MLCK and ROCK did not significantly reduce the intensity of  
216 tissue contraction in any organ examined (Fig. 5 and Movie S10) ( $P > 0.05$ , one-way ANOVA,  $n =$   
217 4). This is in contrast to a previous study, which scored contraction based on basal cell morphology  
218 in mammary tissue treated prior to fixation with this ROCKi (43). When tissue was incubated with  
219 a cocktail of pharmacological inhibitors against MLCK, ROCK, protein kinase C (PKC) (44) and  
220  $\text{Ca}^{2+}$ /calmodulin-dependent protein kinase II (CaMKII) (45), however, contraction was robustly  
221 inhibited in uterine, epididymal and bladder preparations ( $53 \pm 13\%$ ,  $69 \pm 12.5\%$  and  $60 \pm 15\%$   
222 reduction respectively,  $P < 0.05$ , one-way ANOVA,  $n = 4$ ), but persisted in the mammary gland (Fig.  
223 5A-B and Movie S10), suggesting that other pathways are responsible for mammary basal cell  
224 contractions or may compensate when these pathways are transiently disrupted.

225

226 It is also conceivable, however, that some pharmacological inhibitors are unable to effectively and  
227 consistently bind to their intracellular targets when applied to intact, lipid-rich mammary tissue. We  
228 therefore interrogated  $\text{Ca}^{2+}$ -contraction coupling in dissociated primary mammary basal cells in a  
229 2D assay. Cells from pregnant *GCaMP6f-TdTom;K5CreERT2* mice were isolated, plated in co-  
230 culture on a nanopatterned surface (see SI Appendix, Fig. S11B) and imaged within 12 h of  
231 dissection. These conditions were optimal for: 1) maintaining cell health and stage-specific  
232 differentiation; and 2) achieving anisotropy in the arrangement of contractile elements for the  
233 experimental measurement of force generation along a single axis (46). Under these conditions,  
234 OT stimulation produced  $[\text{Ca}^{2+}]_i$  responses, which were coupled to contraction at the first (InsP3)  
235 phase (see SI Appendix, Fig. S11C and Movie S11). Later phase  $\text{Ca}^{2+}$ -contraction coupling,  
236 however, was not able to be assessed in this model, due to the intensity of the first contraction  
237 (even at pM concentrations of OT) and the relatively low strength of the newly formed surface  
238 adhesions (22). Nevertheless, as  $\text{Ca}^{2+}$ -contraction coupling is observed at this phase, we  
239 proceeded to use this system to examine this initial event in primary cells.

240

241 Intracellular  $\text{Ca}^{2+}$  chelation with BAPTA completely blocked  $[\text{Ca}^{2+}]_i$  responses to OT (see SI  
242 Appendix, Fig. S11D and Movie S12). Cell contractions were also attenuated demonstrating,  
243 unequivocally, their  $\text{Ca}^{2+}$ -dependence. To gauge the distance between the  $\text{Ca}^{2+}$  source (in this case  
244 InsP3 receptors) and sensor, we compared OT-mediated basal cell contractions in cells loaded  
245 with two different  $[\text{Ca}^{2+}]_i$  chelators (BAPTA-AM and EGTA-AM), with different  $\text{Ca}^{2+}$  binding rates  
246 but comparable binding affinities (47, 48). Both intracellular BAPTA and EGTA were able to capture

247  $\text{Ca}^{2+}$  between the channel and the sensor (see SI Appendix, Fig. S11D), suggestive of “loose”  $\text{Ca}^{2+}$ -  
248 contraction coupling in these cells that is not strictly dependent on nanodomain signaling (where  
249 EGTA is ineffective) (48). Similar to whole tissue preparations, however, treatment of cells with  
250 MLCK and ROCK inhibitors failed to block OT-mediated basal cell contraction (see SI Appendix,  
251 Fig. S11D). These data are not dissimilar to previous studies, where *in vitro* contraction was  
252 inhibited by only 30% in basal cells isolated from mice deficient for the gene encoding smooth  
253 muscle actin (42) and support a level of functional redundancy in the mammary contraction  
254 pathway.

255

### 256 **Coupled oscillator-based synchronization in the mammary gland**

257  $\text{Ca}^{2+}$ -activation mechanisms in smooth muscle cells are incredibly diverse and are uniquely  
258 adapted to match the developmental stage-specific function of the biological structure on which  
259 they exert their force. Additional complexity arises when the mechanisms responsible for  
260 generating and propagating  $[\text{Ca}^{2+}]_i$  signals in “smooth muscle-like” epithelial lineages are  
261 considered (49). Here, we demonstrate in mammary basal cells that OXTR engagement produces  
262 initial release of  $\text{Ca}^{2+}$  from intracellular stores, sufficient to generate cell and tissue contraction.  
263 Initial  $[\text{Ca}^{2+}]_i$  responses have been shown to be sensitive to PLC inhibition in *in vitro* assays (22)  
264 and similar  $[\text{Ca}^{2+}]_i$  responses are observed with InsP3 infusion (22), consistent with coupling via  
265  $G_q$ -proteins to PLC $\beta$  (18). In some smooth muscle cells,  $[\text{Ca}^{2+}]_i$  signals are propagated along the  
266 length of the cell via the regenerative release of stored  $\text{Ca}^{2+}$  by ryanodine receptors (RYRs) (50,  
267 51). As cytosolic  $\text{Ca}^{2+}$  waves were also observed in mammary basal cells (Fig. 2A), we investigated  
268 novel roles for RYRs in this tissue. *Ryr1* (but not -2 or -3) was expressed in lysates that were  
269 prepared from homogenized mammary tissue during lactation (see SI Appendix, Fig. S12A) and  
270 was enriched in functionally mature basal cells (see SI Appendix, Fig. S12B). To determine the role  
271 of RYR1 channels in these cells, we treated mammary tissue from *GCaMP6f-TdTom;K5CreERT2*  
272 mice with the ryanodine receptor inhibitor dantrolene (52). Dantrolene did not inhibit the initial  
273 release of  $\text{Ca}^{2+}$  from intracellular stores (Fig. 6A temporal sequence 1 and Movie S13). However,  
274 to our surprise,  $[\text{Ca}^{2+}]_i$  oscillations became entrained in some regions and tissue exhibited rhythmic  
275 and sustained pulses of activity that resembled smooth muscle phase waves, with a periodicity  
276 (time between waves) of  $104.2 \pm 16.38$  s and a velocity (speed of wave through the tissue) of  $10.62$   
277  $\pm 2.64 \mu\text{m}\cdot\text{s}^{-1}$  (Fig. 6A temporal sequence 2, Fig. 6B and Movie S13). A similar effect was observed  
278 with inhibiting concentrations of the plant alkaloid ryanodine (53) (Movie S14). These data, together  
279 with our observation that  $[\text{Ca}^{2+}]_i$  oscillations could be temporarily entrained under physiological  
280 conditions (Fig. 3C and see SI Appendix, Fig. S4 and Movies S2 and S6), support a model whereby  
281 mammary basal cells can alternate between unsynchronized movements and coupled oscillator-  
282 based lobuloalveolar synchronization, modulated in-part by the mechanism of ER  $\text{Ca}^{2+}$  release.

283

284 A key factor of coupled oscillator-based synchronization is intercellular communication via gap  
285 junctions (50, 54). Mammary basal cells express Cx43 (55, 56) and mice with severely  
286 compromised Cx43 function have impaired milk ejection (57). However, it is often difficult to  
287 appreciate how stellate basal cells are physically coupled to their neighbors when visualized using  
288 thin tissue sections (see SI Appendix, Fig. S13). Similarly, due to their size and exclusion from near  
289 plasma membrane domains, the true extent of basal cell connectivity has not yet been captured  
290 using 3-dimensional imaging of conventional basal cell markers (see SI Appendix, Fig. S1A). To  
291 overcome this, we developed mice that express a membrane localized fluorescent protein in basal  
292 cells and assessed Cx43 localization in optically cleared tissue. Using this approach, basal cell  
293 boundaries were readily identified, enabling us to visualize how thin processes of adjacent cells are  
294 physically connected (Fig. 6C, top panel). Cx43 was enriched at sites of homotypic cell contact  
295 (Fig. 6C, bottom panel arrows). These data confirm that the cytoplasm of adjacent basal cells are  
296 linked, enabling individual cells to coordinate the activity of the larger system.

297

298 In other tissue types that exhibit rhythmic contractions, e.g., vascular, lymphatic and airway smooth  
299 muscle, periodic release of  $\text{Ca}^{2+}$  from the ER produces membrane depolarization and activation of  
300 L-type  $\text{Ca}^{2+}$  channels (50). Current flow through gap junctions enables depolarization to spread  
301 rapidly into neighboring cells, synchronizing large numbers of cells potentially over millimeter  
302 distances (50, 54). To determine whether L-type calcium channels are involved in synchronization  
303 events in the mammary gland, we treated rhythmically contracting tissue with the L-type  $\text{Ca}^{2+}$   
304 channel blocker nifedipine. Nifedipine rapidly and consistently resulted in the reversion to stochastic  
305 activity [Fig. 6D (absence of repeated sequences of activation for temporal sequence 3) and Movie  
306 S15]. Collectively, these data reveal that mammary basal cells are physically and electrically  
307 coupled, enabling  $\text{Ca}^{2+}$  to control both the behavior of individual cells as well as the system as a  
308 whole.

309

## 310 **Discussion**

311 Real-time, *in situ* activity monitoring provides important insights into how individual cells behave in  
312 multi-dimensional and multi-cellular environments (12–15). This approach was used to describe  
313 and quantify the mechanism by which milk is transported through the hollow mammary epithelium,  
314 making it available on-demand and with minimal delay to the nursing neonate (2, 18). Our data  
315 support a number of novel conclusions that could not have been obtained using conventional  
316 methods.

317

318 Firstly, we revealed that transient  $[Ca^{2+}]_i$  elevations precede and are required for basal cell  
319 contractions in the functionally-mature gland. We extended this finding to demonstrate how  $Ca^{2+}$ -  
320 contraction coupling in a single basal cell can physically warp the layer of alveolar luminal cells that  
321 it encircles. Structure, function and expression were examined in the adjoining ductal epithelium,  
322 previously relegated to a role akin to a biological drinking straw. Instead, our analyses revealed  
323 active participation of the ductal epithelium in the process of milk ejection. Differences in the type  
324 of motion generated by basal cell contractions in ducts and alveoli were ascribed to heterogeneity  
325 in cellular organization, rather than expression or function of contractile elements.

326

327 We explored components of the contractile network downstream of  $Ca^{2+}$  activation in mammary  
328 basal cells. A pattern of pMLC positivity was observed in mammary cell ensembles, which mirrored  
329 the  $Ca^{2+}$  activity of the tissue. Pharmacological inhibition of the  $Ca^{2+}$ -dependent MLCK and the  
330  $Ca^{2+}$ -sensitizer ROCK, however, failed to block mammary contractions in our study. Whilst MLCK  
331 is widely considered to be the primary  $Ca^{2+}$ -dependent regulator of MLC phosphorylation in smooth  
332 muscle, this model is based on reductionist principles, does not fit all smooth muscle cell types and  
333 fails to acknowledge the growing complexity in regulatory kinases known or hypothesized to govern  
334 smooth muscle contraction *in vivo* (58–60). Indeed, embryonic blood vessels from MLCK knockout  
335 mice remain responsive to cytosolic  $Ca^{2+}$  elevations (61). Our data reveal that, similar to aortic  
336 smooth muscle cells, “smooth muscle-like” epithelial cells in the mammary gland also display  
337 considerable complexity and diversity in their biomechanical behavior. Complexity in the pathways  
338 downstream of  $Ca^{2+}$  activation may extend beyond  $Ca^{2+}$ -contraction coupling to  $Ca^{2+}$ -transcription  
339 coupling (62), an aspect of signaling that has not been considered here but which may be relevant  
340 for the interpretation of genetic knockout models (19).

341

342 In addition to the diversity in signal transduction downstream of  $Ca^{2+}$  activation in mammary basal  
343 cells, our study and others (19, 22, 63) have demonstrated that a number of  $Ca^{2+}$  channels—with  
344 distinct activation mechanisms and cellular localizations—participate in its encoding. These include  
345 channels that regulate  $Ca^{2+}$  release from intracellular stores, influx from the extracellular  
346 environment and movement between the cytosol of adjacent cells. In this sense,  $[Ca^{2+}]_i$  acts as a  
347 central node in a type of bow-tie motif in basal cells (64), whereby multiplicity in its encoding and  
348 decoding enable this evolutionarily essential organ to engage local and global motions to ensure  
349 adequate nutrition for the dependent offspring, while on-the-other-hand remaining vulnerable at this  
350 crucial point of convergence.

351

352 The dynamic nature of the oscillatory  $Ca^{2+}$  signal enables basal cells to rapidly cycle between  
353 contracted and relaxed states. We posit that the spatiotemporal properties of this signal are

354 important insomuch as its oscillation intensity and interval match the activation threshold and decay  
355 rate of the downstream effector to permit efficient switching between cycles of contraction and  
356 relaxation. Coupling of the  $\text{Ca}^{2+}$  sensor within nanometer distance to the channel pore, however,  
357 appears unlikely based on the following new observations: 1) both ER  $\text{Ca}^{2+}$  release and  
358 plasmalemmal  $\text{Ca}^{2+}$  influx were sufficient for *in situ* basal cells to develop and bear tension; and 2)  
359 BAPTA-AM and EGTA-AM were equally effective in inhibiting *in vitro* contractions, despite EGTA's  
360 slower binding kinetics. Although not essential for  $\text{Ca}^{2+}$ -contraction coupling, highly spatially  
361 regulated  $[\text{Ca}^{2+}]_i$  signals may be an important factor for  $\text{Ca}^{2+}$ -transcription coupling for the long-term  
362 maintenance of the contractile phenotype (62) or  $\text{Ca}^{2+}$  wave generation at the tissue-level.

363

364 Finally, our data, together with published work, suggests that mammary basal cells are able to shift  
365 between store- (19) and voltage-dependent modes of operation, a phenomenon that appears to be  
366 moderated, at least in-part, by the mechanism of ER  $\text{Ca}^{2+}$  release. It is currently unclear how basal  
367 cells coordinate the activity of these two, often reciprocally regulated (65, 66), influx pathways under  
368 physiological conditions. However, our observation that pharmacological inhibition of RYR1  
369 promoted dihydropyridine-sensitive signal synchronization, corresponds with accounts of RYR  
370 activity in bona fide smooth muscle cells (62). Here, RYR-mediated  $\text{Ca}^{2+}$  sparks can activate nearby  
371  $\text{BK}_{\text{Ca}}$  channels, producing spontaneous transient outward currents (STOCs), membrane  
372 hyperpolarization and reduced  $\text{Ca}_v1.2$  activity (50, 62). Optical monitoring of voltage in 3-  
373 dimensions using genetically-encoded voltage indicators (GEVIs) (67) and examination of  
374 population dynamics in *Cacna1c*-, *Ryr1*- and *Kcnma1*- conditional knockout mice remain aims for  
375 the future. It is also unclear at this time whether spatial synchronicity can be initiated by any  
376 oscillating basal cell (alveolar or ductal) within the mammary epithelium or whether basal cells lock  
377 into the frequency of a putative population of epithelial (68) or interstitial (69) mammary  
378 "pacemaker" cells. This question may be addressed by future studies using light-sheet fluorescence  
379 microscopy and quantitative image analysis to create a spatial footprint of the frequency dynamics  
380 of individual oscillators and phase advanced cells.

381

382 In summary, by imaging activity in the mammary gland across scales, we were able to visualize  
383 and describe in unprecedented detail how the repetitive and collective effort of thousands of  
384 mammary basal cells facilitate the transport of a thick biological emulsion through a narrow passage  
385 in a manner that is both consistent and persistent. Moreover, the system presented here represents  
386 a novel, physiologically relevant model for studying the collective nature of mammalian biological  
387 processes.

388

389

390 **Materials and Methods**

391

392 Mice

393 Animal experimentation was carried out in accordance with the *Australian Code for the Care and*  
394 *Use of Animals for Scientific Purposes* and the *Queensland Animal Care and Protection Act (2001)*,  
395 with local animal ethics committee approval. Strain, genotyping and reporter induction methods  
396 detailed in SI Appendix.

397

398 Human subjects

399 Healthy tissue biopsies from consented lactating women were obtained from the Susan G. Komen  
400 Tissue Bank at the IU Simon Cancer Center, see SI Appendix.

401

402 Ex vivo tissue imaging

403 Mammary glands and uteri were harvested from lactating wildtype, *GCaMP6f;K5CreERT2* or  
404 *GCaMP6f-TdTom;K5CreERT2* mice, diced into 3-4 mm<sup>3</sup> pieces and loaded with CellTracker™ (1.5  
405 μM) in complete media for at least 20 min at 37°C and 5% CO<sub>2</sub> (19). Under these conditions  
406 CellTracker™ preferentially labels luminal cells (see SI Appendix, Fig. S1A). Images were acquired  
407 using an Olympus FV3000 LSM; see SI Appendix for details and intravital imaging conditions.

408

409 Statistical analysis

410 Statistical analysis was performed in GraphPad Prism (v7.03). Details of statistical tests are  
411 outlined in figure legends.

412

413 Data availability

414 All data are available in the paper. Scripts are available on GitHub.

415

416 **Acknowledgments**

417 This work was supported by the National Health and Medical Research Council (1141008,  
418 1138214), University of Queensland, the Mater Foundation (Equity Trustees / AE Hingeley Trust)  
419 and the National Stem Cell Foundation of Australia. We thank Dr. Jerome Boulanger for the 3D  
420 denoising algorithm and Mr Karsten Bach for assistance with accessing and analyzing RNAseq  
421 data. Samples from the Komen Tissue Bank at the IU Simon Cancer Center were used in this study;  
422 we thank contributors, donors and their families.



## References

- 423 1. Victora CG, et al. (2016) Breastfeeding in the 21st century: Epidemiology, mechanisms,  
424 and lifelong effect. *Lancet* 387(10017):475–490.
- 425 2. Macias H, Hinck L (2012) Mammary gland development. *Wiley Interdiscip Rev Dev Biol*  
426 1(4):533–557.
- 427 3. Cowin P, Wysolmerski J (2010) Molecular mechanisms guiding embryonic mammary  
428 gland development. *Cold Spring Harb Perspect Biol* 2(6):a003251.
- 429 4. Lloyd-Lewis B, Harris OB, Watson CJ, Davis FM (2017) Mammary stem cells: Premise,  
430 properties and perspectives. *Trends Cell Biol* 8:556–567.
- 431 5. Sleeman KE, et al. (2007) Dissociation of estrogen receptor expression and in vivo stem  
432 cell activity in the mammary gland. *J Cell Biol* 176(1):19–26.
- 433 6. Van Keymeulen A, et al. (2017) Lineage-restricted mammary stem cells sustain the  
434 development, homeostasis, and regeneration of the estrogen receptor positive lineage.  
435 *Cell Rep* 20(7):1525–1532.
- 436 7. Bach K, et al. (2017) Differentiation dynamics of mammary epithelial cells revealed by  
437 single-cell RNA sequencing. *Nat Commun* 8:2128.
- 438 8. Van Keymeulen A, et al. (2011) Distinct stem cells contribute to mammary gland  
439 development and maintenance. *Nature* 479(7372):189–193.
- 440 9. Lloyd-Lewis B, Davis FM, Harris OB, Hitchcock JR, Watson CJ (2018) Neutral lineage  
441 tracing of proliferative embryonic and adultmammary stem/progenitor cells. *Development*  
442 145(14):164079.
- 443 10. Davis FM, et al. (2016) Single-cell lineage tracing in the mammary gland reveals  
444 stochastic clonal dispersion of stem/progenitor cell progeny. *Nat Commun* 7:13053.
- 445 11. Gjorevski N, Nelson CM (2011) Integrated morphodynamic signalling of the mammary  
446 gland. *Nat Rev Mol Cell Biol* 12(9):581–593.
- 447 12. Toyota M, et al. (2018) Glutamate triggers long-distance, calcium-based plant defense  
448 signaling. *Science* 361(6407):1112–1115.
- 449 13. Heap LAL, Vanwalleghem G, Thompson AW, Favre-Bulle IA, Scott EK (2018) Luminance  
450 changes drive directional startle through a thalamic pathway. *Neuron* 99:293–301.
- 451 14. Dunn TW, et al. (2016) Neural circuits underlying visually evoked escapes in larval  
452 zebrafish. *Neuron* 89(3):613–628.
- 453 15. Cichon J, Gan WB (2015) Branch-specific dendritic Ca<sup>2+</sup> spikes cause persistent synaptic  
454 plasticity. *Nature* 9(520):180–5.
- 455 16. Chen T-W, et al. (2013) Ultrasensitive fluorescent proteins for imaging neuronal activity.  
456 *Nature* 499(7458):295–300.
- 457 17. Chen Q, et al. (2012) Imaging neural activity using Thy1-GCaMP transgenic mice. *Neuron*

- 458 76:297–308.
- 459 18. Gimpl G, Fahrenholz F (2001) The oxytocin receptor system: structure, function, and  
460 regulation. *Physiol Rev* 81:629–683.
- 461 19. Davis FM, et al. (2015) Essential role of Orai1 store-operated calcium channels in  
462 lactation. *Proc Natl Acad Sci* 112(18):5827–5832.
- 463 20. Moore DM, Vogl AW, Baimbridge K, Emerman JT (1987) Effect of calcium on oxytocin-  
464 induced contraction of mammary gland myoepithelium as visualized by NBD-phalloidin. *J*  
465 *Cell Sci* 88:563–569.
- 466 21. Olins GM, Bremel RD (1984) Oxytocin-stimulated myosin phosphorylation in mammary  
467 myoepithelial cells: Roles of calcium ions and cyclic nucleotides. *Endocrinology*  
468 114(5):1617–1626.
- 469 22. Nakano H, Furuya K, Yamagishi S (2001) Synergistic effects of ATP on oxytocin-induced  
470 intracellular Ca<sup>2+</sup> response in mouse mammary myoepithelial cells. *Pflugers Arch Eur J*  
471 *Physiol* 442(1):57–63.
- 472 23. Lee HJ, Caldwell HK, Macbeth AH, Tolu SG, Young WS (2008) A conditional knockout  
473 mouse line of the oxytocin receptor. *Endocrinology* 149(7):3256–63.
- 474 24. Nishimori K, et al. (1996) Oxytocin is required for nursing but is not essential for parturition  
475 or reproductive behavior. *Proc Natl Acad Sci U S A* 93:11699–11704.
- 476 25. Takayanagi Y, et al. (2005) Pervasive social deficits, but normal parturition, in oxytocin  
477 receptor-deficient mice. *Proc Natl Acad Sci U S A* 102(44):16096–101.
- 478 26. Dana H, et al. (2018) High-performance GFP-based calcium indicators for imaging activity  
479 in neuronal populations and microcompartments. *bioRxiv*:434589.
- 480 27. Srinivasan R, et al. (2016) New transgenic mouse lines for selectively targeting astrocytes  
481 and studying calcium signals in astrocyte processes in situ and in vivo. *Neuron*  
482 92(6):1181–1195.
- 483 28. Lloyd-Lewis B, et al. (2016) Imaging the mammary gland and mammary tumours in 3D:  
484 Optical tissue clearing and immunofluorescence methods. *Breast Cancer Res* 18(1).
- 485 29. Akemann W, Mutoh H, Perron A, Rossier J, Knöpfel T (2010) Imaging brain electric  
486 signals with genetically targeted voltage-sensitive fluorescent proteins. *Nat Methods*  
487 7:643–9.
- 488 30. Dupont G, Combettes L, Bird GS, Putney JW (2011) Calcium oscillations. *Cold Spring*  
489 *Harb Perspect Biol* 3(3):a004226.
- 490 31. Masedunskas A, Chena Y, Stussman R, Weigert R, Mather IH (2017) Kinetics of milk lipid  
491 droplet transport, growth, and secretion revealed by intravital imaging: Lipid droplet  
492 release is intermittently stimulated by oxytocin. *Mol Biol Cell* 28:935–946.
- 493 32. Avants BB, et al. (2011) A reproducible evaluation of ANTs similarity metric performance

- 494 in brain image registration. *Neuroimage* 54(3):2033–44.
- 495 33. Avants BB, Epstein C, Grossman M, Gee JC (2008) Symmetric diffeomorphic image  
496 registration with cross-correlation: evaluating automated labeling of elderly and  
497 neurodegenerative brain. *Med Image Anal* 12(1):26–41.
- 498 34. Dong TX, et al. (2017) T-cell calcium dynamics visualized in a ratiometric tdTomato-  
499 GCaMP6f transgenic reporter mouse. *Elife*. doi:10.7554/eLife.32417.
- 500 35. Moumen M, et al. (2011) The mammary myoepithelial cell. *Int J Dev Biol*.  
501 doi:10.1387/ijdb.113385mm.
- 502 36. Stožer A, et al. (2013) Functional connectivity in islets of Langerhans from mouse  
503 pancreas tissue slices. *PLoS Comput Biol* 9(2):e1002923.
- 504 37. Watts DJ, Strogatz SH (1998) Collective dynamics of “small-world” networks. *Nature*  
505 393(6684):440–2.
- 506 38. Farmer DT, et al. (2017) Defining epithelial cell dynamics and lineage relationships in the  
507 developing lacrimal gland. *Development* 144(13):2517–2528.
- 508 39. Hawley D, et al. (2018) Myoepithelial cell-driven acini contraction in response to oxytocin  
509 receptor stimulation is impaired in lacrimal glands of Sjögren’s syndrome animal models.  
510 *Sci Rep* 8(1):9919.
- 511 40. Thackare H, Nicholson HD, Whittington K (2006) Oxytocin - Its role in male reproduction  
512 and new potential therapeutic uses. *Hum Reprod Update* 12(4):437–48.
- 513 41. Arrighi S (2014) Are the basal cells of the mammalian epididymis still an enigma? *Reprod*  
514 *Fertil Dev* 26(8):1061–71.
- 515 42. Haaksma CJ, Schwartz RJ, Tomasek JJ (2011) Myoepithelial cell contraction and milk  
516 ejection are impaired in mammary glands of mice lacking smooth muscle alpha-actin. *Biol*  
517 *Reprod* 85:13–21.
- 518 43. Raymond K, et al. (2011) Control of mammary myoepithelial cell contractile function by  
519  $\alpha 3\beta 1$  integrin signalling. *EMBO J* 30:1896–1906.
- 520 44. Kuo IY, Ehrlich BE (2015) Signaling in muscle contraction. *Cold Spring Harb Perspect Biol*  
521 7:a006023.
- 522 45. Rokolya A, Singer HA (2000) Inhibition of CaM kinase II activation and force maintenance  
523 by KN-93 in arterial smooth muscle. *Am J Physiol - Cell Physiol* 278:C537-45.
- 524 46. Chaterji S, et al. (2014) Synergistic effects of matrix nanotopography and stiffness on  
525 vascular smooth muscle cell function. *Tissue Eng Part A* 20(15–16):2115–26.
- 526 47. Vyleta NP, Jonas P (2014) Loose coupling between Ca<sup>2+</sup> channels and release sensors  
527 at a plastic hippocampal synapse. *Science* 343(6171):665–70.
- 528 48. Eggermann E, Bucurenciu I, Goswami SP, Jonas P (2012) Nanodomain coupling between  
529 Ca<sup>2+</sup> channels and sensors of exocytosis at fast mammalian synapses. *Nat Rev*

- 530           *Neurosci* 13:7–21.
- 531   49.   Richardson KC (2009) Contractile tissues in the mammary gland, with special reference to  
532           myoepithelium in the goat. *J Mammary Gland Biol Neoplasia* 136(882):30–45.
- 533   50.   Berridge MJ (2008) Smooth muscle cell calcium activation mechanisms. *J Physiol*  
534           586(21):5047–61.
- 535   51.   Collier ML, Ji G, Wang YX, Kotlikoff MI (2000) Calcium-induced calcium release in smooth  
536           muscle: Loose coupling between the action potential and calcium release. *J Gen Physiol*  
537           115(5):653–62.
- 538   52.   Choi RH, Koenig X, Launikonis BS (2017) Dantrolene requires Mg<sup>2+</sup> to arrest malignant  
539           hyperthermia. *Proc Natl Acad Sci U S A* 114(18):4811–5.
- 540   53.   Meissner G (1986) Ryanodine activation and inhibition of the Ca<sup>2+</sup> release channel of  
541           sarcoplasmic reticulum. *J Biol Chem* 261(14):6300–6.
- 542   54.   Imtiaz MS, Von Der Weid PY, Van Helden DF (2010) Synchronization of Ca<sup>2+</sup>  
543           oscillations: A coupled oscillator-based mechanism in smooth muscle. *FEBS J* 277:278–  
544           85.
- 545   55.   Mroue R, Inman J, Mott J, Budunova I, Bissell MJ (2015) Asymmetric expression of  
546           connexins between luminal epithelial- and myoepithelial- cells is essential for contractile  
547           function of the mammary gland. *Dev Biol* 399(1):15–26.
- 548   56.   Talhok RS, et al. (2005) Developmental expression patterns and regulation of connexins  
549           in the mouse mammary gland: Expression of connexin30 in lactogenesis. *Cell Tissue Res*  
550           19:49–59.
- 551   57.   Stewart MKG, et al. (2013) The severity of mammary gland developmental defects is  
552           linked to the overall functional status of Cx43 as revealed by genetically modified mice.  
553           *Biochem J* 449:401–413.
- 554   58.   Ratz PH (2013) Inhibitor κB Kinase: Another node in the cell signaling network regulating  
555           smooth muscle contraction. *Circ Res* 113(5):484–6.
- 556   59.   Ying Z, et al. (2013) Inhibitor κB Kinase 2 Is a Myosin Light Chain Kinase in Vascular  
557           Smooth Muscle. *Circ Res* 113(5):562–70.
- 558   60.   Artamonov M V., et al. (2018) RSK2 contributes to myogenic vasoconstriction of  
559           resistance arteries by activating smooth muscle myosin and the Na<sup>+</sup>/H<sup>+</sup> exchanger. *Sci*  
560           *Signal* 11(554):eaar3924.
- 561   61.   Somlyo AV, et al. (2004) Myosin Light Chain Kinase Knockout. *J Muscle Res Cell Motil.*  
562           doi:10.1023/b:jure.0000038362.84697.c0.
- 563   62.   Hill-Eubanks DC, Werner ME, Heppner TJ, Nelson MT (2011) Calcium signaling in smooth  
564           muscle. *Cold Spring Harb Perspect Biol* 3(9):a004549.
- 565   63.   Nakano H, Furuya K, Furuya S, Yamagishi S (1997) Involvement of P2-purinergic

- 566 receptors in intracellular Ca<sup>2+</sup> responses and the contraction of mammary myoepithelial  
567 cells. *Pflugers Arch Eur J Physiol* 435(1):1–8.
- 568 64. Brodskiy PA, Zartman JJ (2018) Calcium as a signal integrator in developing epithelial  
569 tissues. *Phys Biol* 15(5):051001.
- 570 65. Wang Y, et al. (2010) The calcium store sensor, STIM1, reciprocally controls Orai and Ca  
571 V1.2 channels. *Science* 330(6000):105–9.
- 572 66. Park CY, Shcheglovitov A, Dolmetsch R (2010) The CRAC channel activator STIM1 binds  
573 and inhibits L-type voltage-gated calcium channels. *Science* 330(6000):101–105.
- 574 67. Villette V, et al. (2019) Ultrafast Two-Photon Imaging of a High-Gain Voltage Indicator in  
575 Awake Behaving Mice. *Cell* 179(7):1590–1608.
- 576 68. De Blasio BF, Iversen JG, Røttingen JA (2004) Intercellular calcium signalling in cultured  
577 renal epithelia: A theoretical study of synchronization mode and pacemaker activity. *Eur*  
578 *Biophys J* 33:657–70.
- 579 69. Gherghiceanu M, Popescu LM (2005) Interstitial Cajal-like cells (ICLC) in human resting  
580 mammary gland stroma. Transmission electron microscope (TEM) identification. *J Cell*  
581 *Mol Med* 9(4):893–910.

## Figures

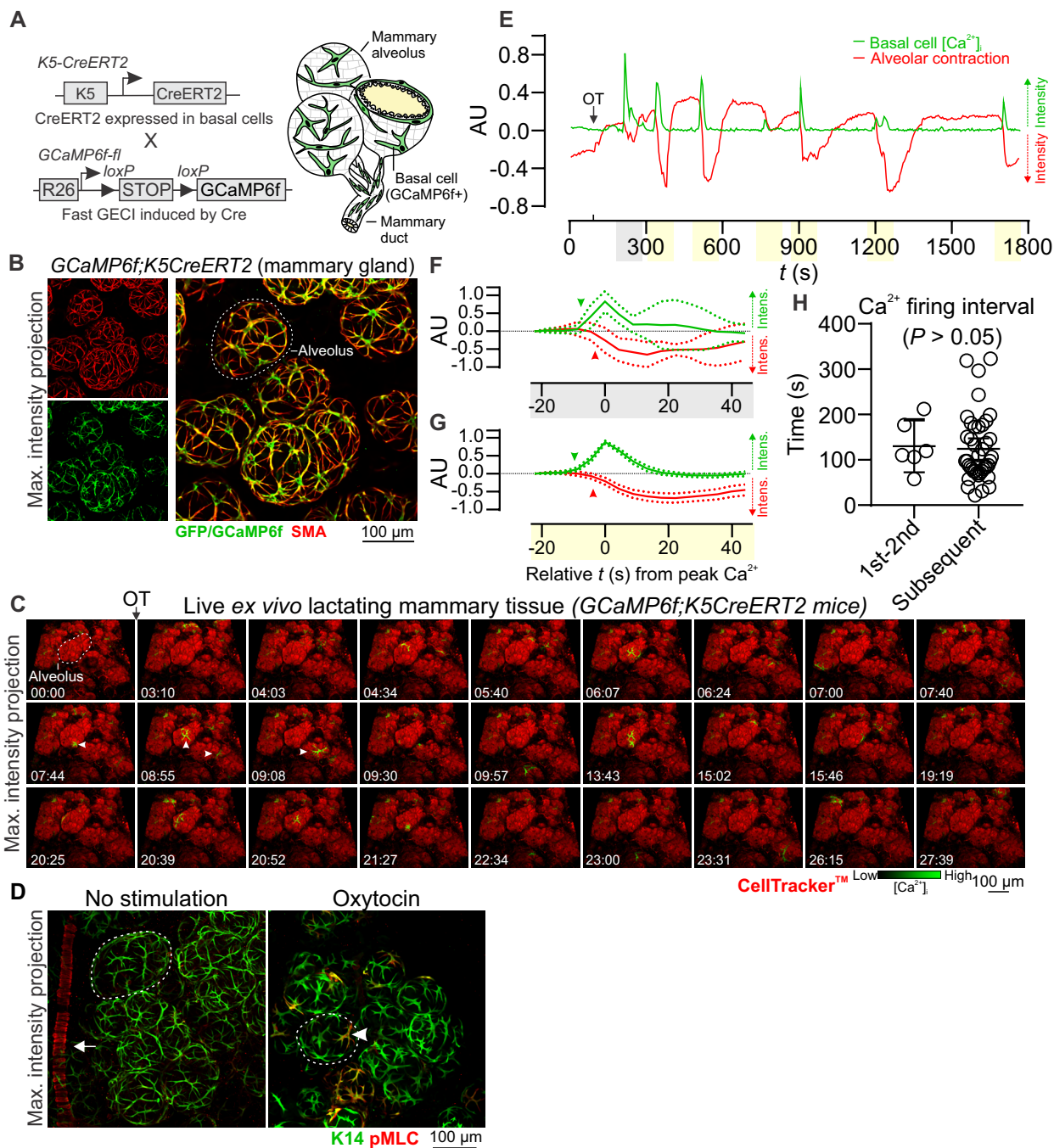


**Figure 1. Basal cell  $\text{Ca}^{2+}$  oscillations precede alveolar contractions.** (A) Schematic representation of *GCaMP6f;K5CreERT2* model. (B) Maximum intensity z-projection of cleared lactating mammary tissue immunostained with smooth muscle actin (SMA) to reveal basal cells and anti-GFP antibody to detect GCaMP6f. (C) 3D time-lapse imaging of live mammary tissue from *GCaMP6f;K5CreERT2* lactating mice stimulated with OT (85 nM) at 01:33 (min:s). Images show maximum intensity z-projection. Arrowheads point to  $\text{Ca}^{2+}$  events in single cells. See Movie S1. (D) Maximum intensity z-projections of cleared mammary tissue immunostained with K14 to reveal basal cells and pMLC to show sites of contractile activity. Arrow shows pMLC<sup>+</sup> blood vessel in control tissue, arrowhead shows pMLC<sup>+</sup> basal cell in tissue stimulated with OT (85 nM) prior to fixation; dotted lines surround alveolar units. (E) Quantification of  $[\text{Ca}^{2+}]_i$  responses (green) and alveolar unit contraction (red) in lactating mammary tissue from *GCaMP6f;K5CreERT2* mice.  $[\text{Ca}^{2+}]_i$  measurements are  $\Delta F/F_0$ . Alveolar unit contractions shown by negative deflections (CellTracker™ fluorescence). (F-G) Average ( $\pm$  SEM) peak  $[\text{Ca}^{2+}]_i$  and contractile responses. Highlighting (x-axis) corresponds with events linked in (E); arrowheads show initiation of the response. (H) Interval between the first-second and all subsequent  $[\text{Ca}^{2+}]_i$  events ( $P > 0.05$ , Student's t-test). AU, arbitrary unit; n = 3 mice.

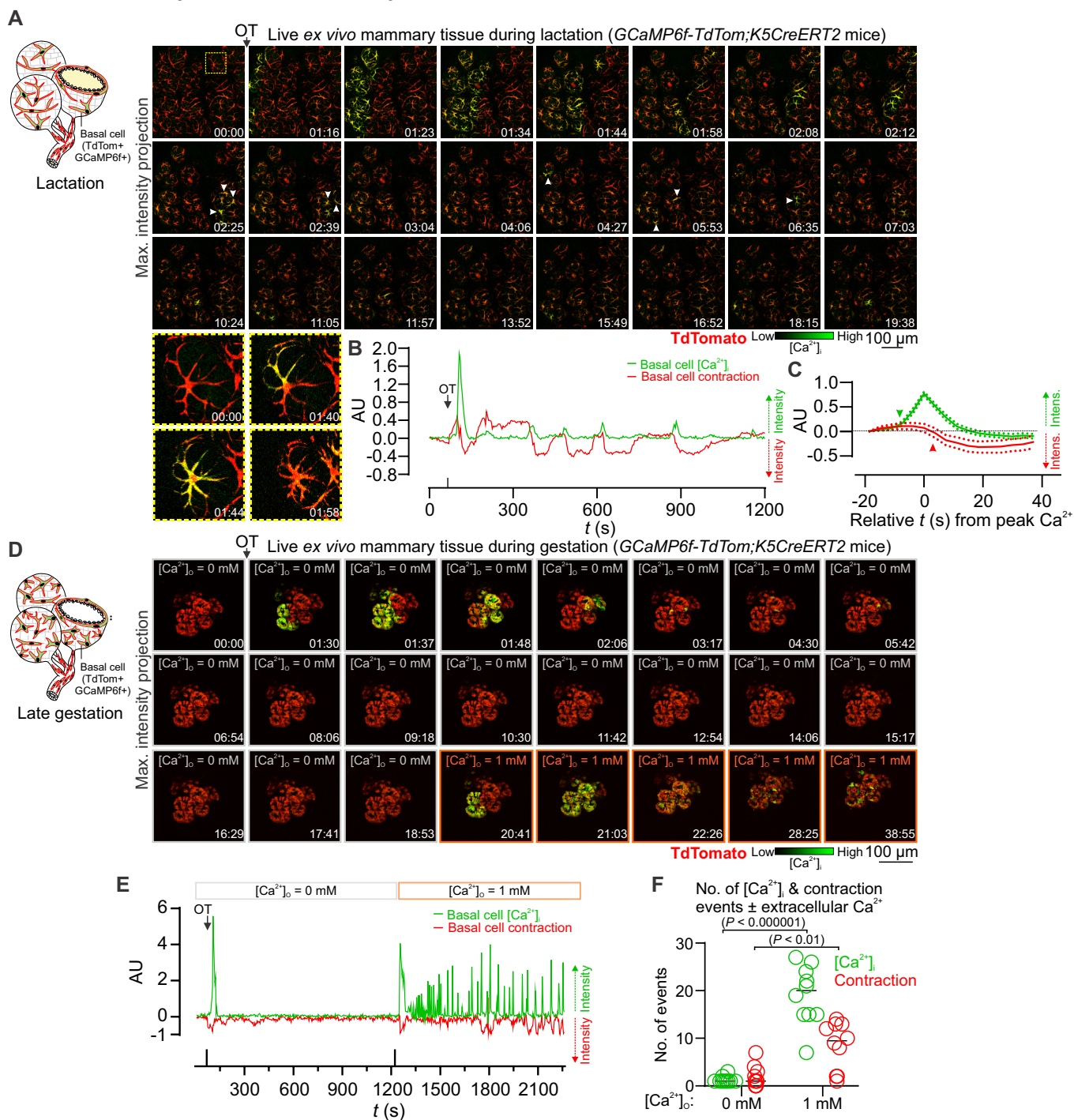




**Figure 2. Ca<sup>2+</sup>-contraction coupling.** (A) 3D time-lapse imaging of live mammary tissue from *GCaMP6f-TdTom;K5CreERT2* mice stimulated with OT (85 nM) at 01:09 (min:s). Images show maximum intensity z-projection. Box (frame 1) expanded in panel below; arrowheads point to Ca<sup>2+</sup> events in single cells. See Movie S3. (B) Quantification of [Ca<sup>2+</sup>]<sub>i</sub> responses (green) and alveolar unit contraction (red) in lactating mammary tissue from *GCaMP6f-TdTom;K5CreERT2* mice. [Ca<sup>2+</sup>]<sub>i</sub> measurements are  $\Delta F/F_0$ . Basal cell contractions shown by negative deflections (TdTomato fluorescence). (C) Average ( $\pm$  SEM) peak [Ca<sup>2+</sup>]<sub>i</sub> response and contractile response in mammary tissue isolated from lactating *GCaMP6f-TdTom;K5CreERT2* mice. Values averaged from both the first response and the oscillatory phase. (D) 3D time-lapse imaging of live mammary tissue from *GCaMP6f-TdTom;K5CreERT2* mice (15.5-16.5 d.p.c., days post coitus) stimulated with OT (85 nM) at 01:08 (min:s) under extracellular Ca<sup>2+</sup> free conditions. Images show maximum intensity z-projection. Ca<sup>2+</sup> (1 mM free Ca<sup>2+</sup>) was added back at 20:23 (min:sec). See Movie S5. (E) Quantification of [Ca<sup>2+</sup>]<sub>i</sub> responses and alveolar unit contraction in mammary tissue from pregnant *GCaMP6f-TdTom;K5CreERT2* mice stimulated with OT under extracellular Ca<sup>2+</sup> free conditions and with Ca<sup>2+</sup> addback. [Ca<sup>2+</sup>]<sub>i</sub> measurements are  $\Delta F/F_0$ . Basal cell contractions shown by negative deflections (TdTomato fluorescence). (F) Number of [Ca<sup>2+</sup>]<sub>i</sub> and contraction events  $\pm$  extracellular Ca<sup>2+</sup> ([Ca<sup>2+</sup>]<sub>o</sub>). Graph shows individual measurements and median. *P* value shown inset from multiple t-tests. N = 3 mice.

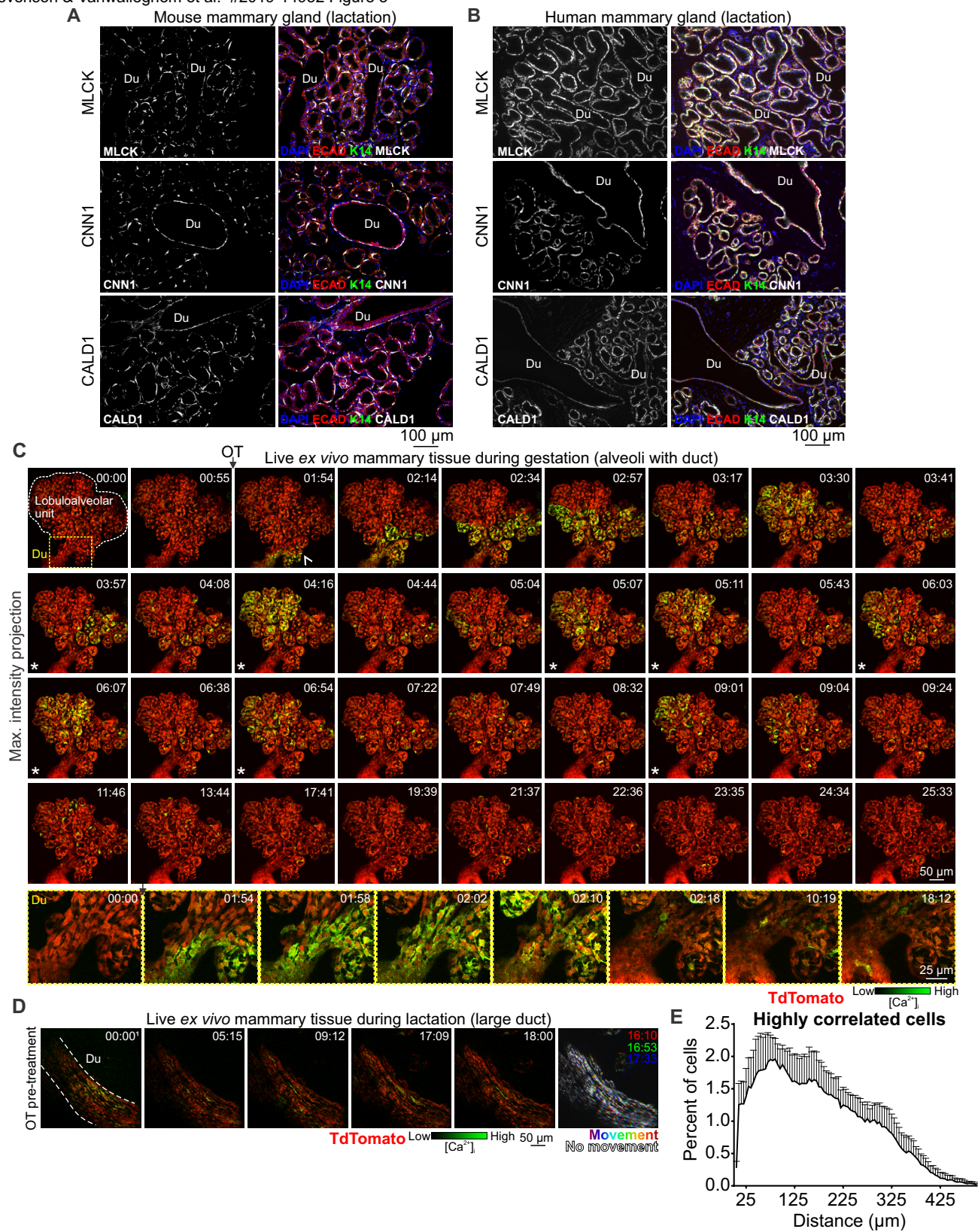


**Figure 3.**

**Functional differentiation and Ca<sup>2+</sup>-contraction coupling in ducts and alveoli. (A-B)** Immunostaining of paraffin embedded mouse and human lactating tissue. MLCK, CNN1 and CALD1 are expressed in both ducts (Du) and alveoli. E-cadherin shows the luminal cell lineage; K14 shows the basal cell lineage. Nuclei are stained with DAPI; n = 3 samples, mouse and human. **(C)** 3D time-lapse imaging of live mammary tissue from a pregnant (15.5-16.5 d.p.c.) *GCaMP6f-TdTom;K5CreERT2* mouse stimulated with OT (85 nM) at 01:15 (min:s). Images show maximum intensity z-projection of live tissue; box (frame 1) shows subtending duct (Du, magnified in bottom panel), extending deeper into the tissue. Arrowhead at 01:54 shows direction of OT diffusion; asterisks show coordinated firing; n = 3. See Movie S6. **(D)** 3D time-lapse imaging of a large duct from a lactating *GCaMP6f-TdTom;K5CreERT2* mouse stimulated with OT (85 nM) immediately prior to<sup>1</sup> imaging. Images show maximum intensity z-projection of live tissue; n = 3. See Movie S7. **(E)** Percent of cells with a high correlation coefficient (> 0.5) in Ca<sup>2+</sup> firing and the Euclidean distance of correlated events. Graph shows average ± SEM (n = 4 mice, gestation).

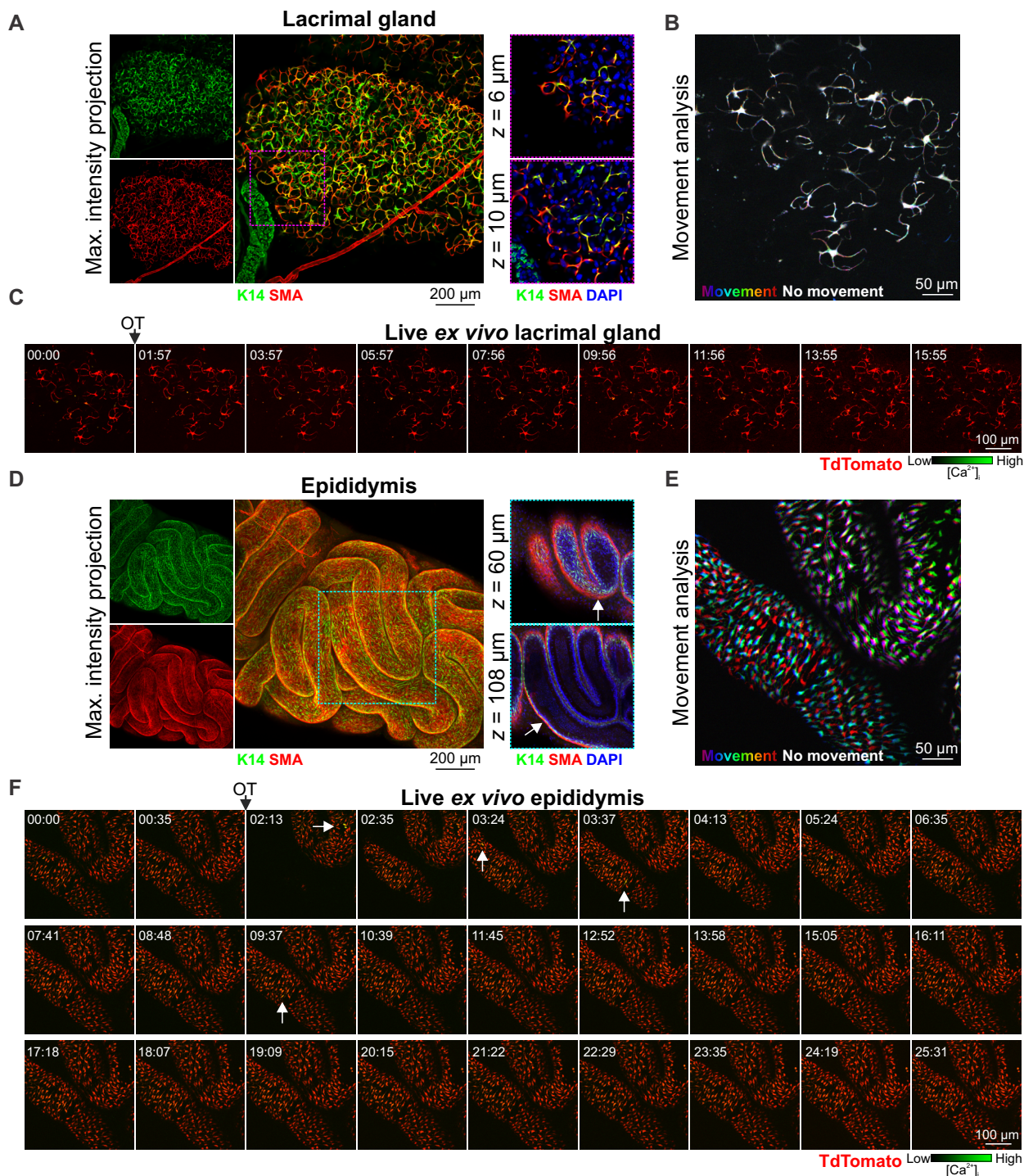


**Figure 4. OT responses in basal epithelial cells of other fluid moving organs. (A)** Maximum intensity z-projection and optical slices of lacrimal tissue. Lacrimal acinar basal cells express K14 and SMA. **(B)** Analysis of tissue movement created by the overlay of 3 images (approx. 43 s apart). Each image has been assigned a primary color. Regions that do not move during the 90 s window have R-G-B pixels superimposed and are white. Regions where significant movement has occurred appear R, G, B or a combination of 2 colors. See Movie S8. **(C)** 3D time-lapse imaging of lacrimal tissue from *GCaMP6f-TdTom;K5CreERT2* mice. Tissue was stimulated with OT (85 nM, 00:45). Image series show maximum intensity z-projection. **(D)** Maximum intensity z-projection and optical slices of cleared mouse epididymis (caput). Basal K14 positive cells are surrounded by SMA positive cells (arrow). **(E)** Tissue movement analysis of 3 images (approx. 45 s apart) as per (B). **(F)** 3D time-lapse imaging of epididymal tissue from *GCaMP6f-TdTom;K5CreERT2* mice. Tissue was stimulated with OT (850 nM, 01:38); arrows show single cell calcium responses. See Movie S9. N = 3 mice.

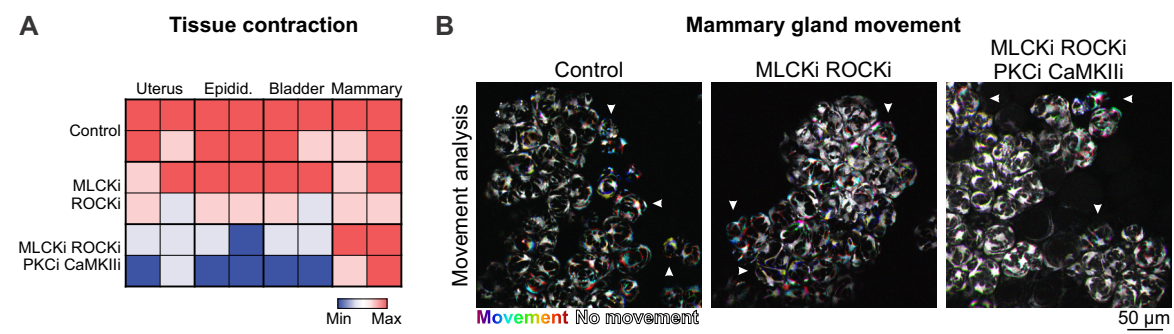


**Figure 5. Pharmacological inhibition of the contractile pathway.** (A) Matrix of contractile activity in tissue pieces isolated from uterus, epididymis, bladder and mammary gland and treated with either buffer (control), a combination of inhibitors of MLCK (ML-9) and ROCK (Y27632) or a combination of inhibitors of MLCK (ML-9), ROCK (Y27632), PKC (calphostin-C) and CaMKII (KN93). Contractions were induced with oxytocin (85 nM, uterus and mammary gland; 850 nM epididymis) or carbachol (10  $\mu$ M, bladder). See Movie S10. (B) Analysis of tissue movement in mammary tissue pieces created by the overlay of 3 images (30 s apart). Each image has been assigned a primary color. Regions that do not move during the 60 s window have R-G-B pixels superimposed and are white. Regions where significant movement has occurred appear R, G, B or a combination of 2 colors. N = 4 mice.

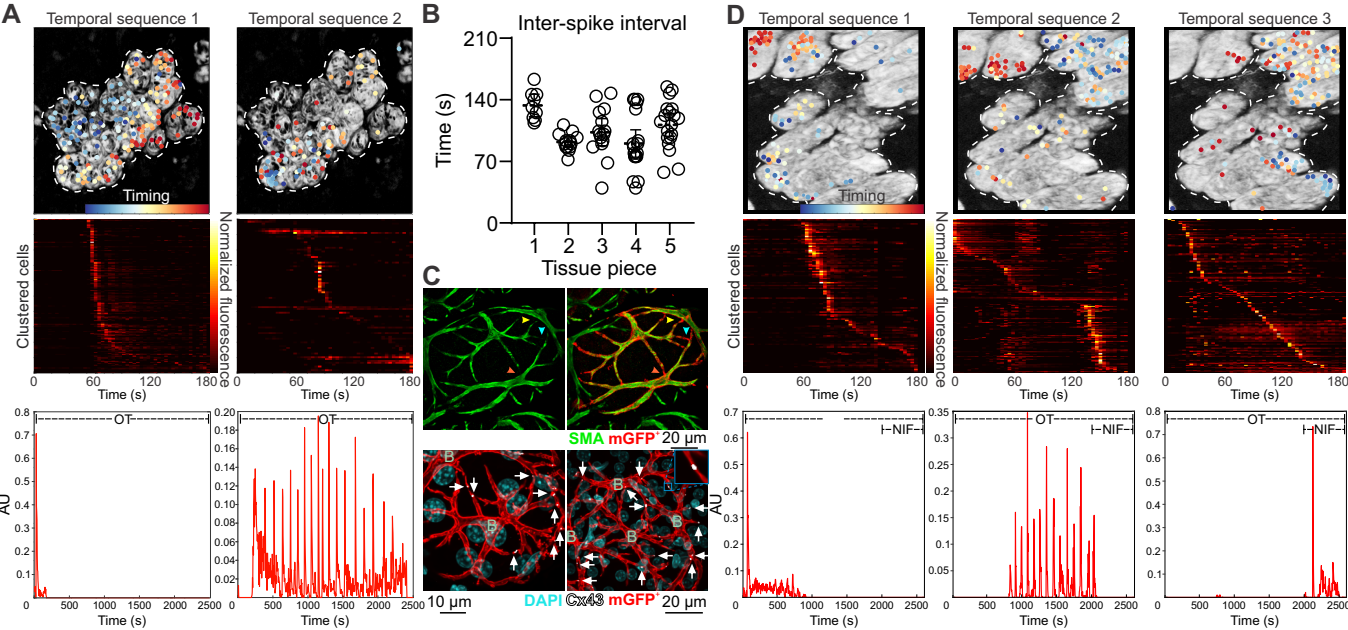




**Figure 6. Dantrolene-induced tissue synchronization.** (A) Sequential Non-Negative Matrix Factorization (seqNMF) was used for unsupervised discovery of repeated temporal sequences of activation and to cluster cells accordingly. Temporal sequence 1 corresponds to the initial InsP3 response, temporal sequence 2 corresponds to the dantrolene dependent synchronized oscillations. Dots (top panel) are cells color-coded (see timing colorbar) according to the order of their activation in the sequence (middle panel, each row is one cell) and overlaid on a maximum intensity z-projection of the green channel. The times at which each temporal sequence of  $[Ca^{2+}]_i$  activity is repeated for each cluster is represented by a spike in the bottom panel; n = 3 mice. (B) Interval between each synchronized oscillation in *ex vivo* dantrolene-treated mammary tissue (mean +/- 95% CI); n = 5 tissue pieces from at least 3 mice. (C) Optically-cleared mammary tissue from lactating mice showing SMA immunostaining (green, top panel) and cells expressing a membrane targeted fluorescent protein (red, top panel). Colored arrowheads point to sites of cell-cell contact that are revealed by the membrane fluorescent protein (Lck-GCaMP6f/mGFP, detected using an anti-GFP antibody). Immunostaining for Cx43 (white, bottom panel) in cells expressing the membrane targeted fluorescent protein (red, bottom panel). White arrows show Cx43 staining at sites where basal cells are connected; B, basal cell; n = 3 mice. (D) seqNMF as in A, where temporal sequence 1 corresponds to the initial InsP3 response, temporal sequence 2 corresponds to dantrolene dependent synchronized oscillations and temporal sequence 3 corresponds to addition of nifedipine. After addition of nifedipine, the synchronized activity disappears and switches to a stochastic activity distributed through the tissue, as can be seen by the lack of repeated spikes in the bottom pane. See Movie S15. N = 3 mice.